This article has been accepted for publication in a future issue of this journal, but has not been fully edited. Content may change prior to final publication. Citation information: DOI 10.1109/TTE.2017.2666554, IEEE Transactions on Transportation Electrification

Sizing of Inductive Power Pads for Dynamic Charging of EVs on IPT Highways

Ganesh R. Nagendra, *Member, IEEE,* Grant A. Covic, *Senior Member, IEEE,* and John T. Boys

***Abstract*—In this paper, the physical sizing of IPT power pads on a dynamic IPT highway is explored. Previous work has focussed only on sizing for stationary IPT chargers, and this paper extends this analysis for Double-D (DD) and Double-D Quadrature (DDQ) based power pads. Firstly, a window function (here fitted using a Gaussian distribution) is created to model the power transfer profiles when individual primary pads on the highway are energised. An analytical expression is developed that can predict the resultant power profiles from energising multiple primary pads, depending on the phase angle between the individual primary pad currents and the physical sizes of the IPT pads. A practical design example is then presented that shows how pads could be sized to allow for 10 kW power transfer to sedans and SUVs (air-gaps ranging from 250-400 mm) with only a 25% reduction in power as they drive along the highway.**

***Index Terms*—Couplers, electric vehicles, inductive power transmission, magnetic analysis, wireless power transfer.**

I. Introduction

MODERN Electric Vehicles (EVs) are fast becoming an attractive transportation alternative to traditional gasoline driven internal combustion engine based vehicles [1]–[5]. If the electricity used to charge these EVs can be generated from renewable sources, then they can significantly reduce our fossil fuel usage as well as global greenhouse gas emissions. Growth in EV sales has risen dramatically over the past few years, with several leading car manufacturers offering EV models as part of their product line. However, as the energy density of battery banks such as Lithium ion (100 - 200 Wh/kg) is significantly lower than that of petrol (12 kWh/kg), EVs have a limited range and need to be frequently recharged [6]. This recharging is often carried out by inserting a connector into a custom plug on the EV body. The other end of this connector may simply be connected directly to a mains power outlet or a dedicated high power charger. This poses an inconvenience to the driver as they have to remember to plug in their EV regularly, and can also pose safety concerns in adverse weather conditions (e.g. snow, rain) due to the high battery bank voltages of approx. 300V.

Inductive Power Transfer or IPT is a means of wirelessly transferring power across an air-gap without the need for direct electrical contact. It relies on the fundamental principles of Ampère's and Faraday's Laws, and offers a clean, reliable, contactless, and safe means for transferring power. Practically, IPT can also allow stationary EVs to be recharged without requiring cumbersome plugs and connectors. Instead, power can be transferred over an air-gap from a primary coil (buried in the ground) to a secondary coil (mounted underneath the EV chassis) to recharge EVs rapidly at rates of 5 - 50 kW [7]–[12]. If IPT systems are incorporated into the highway network, then EVs can even be powered dynamically as they move [13]–[20]. This has the potential of ensuring that EVs have unlimited range capabilities, higher operating efficiencies, reduced battery sizes and cost, as well as shorter dedicated charging times.

One of the challenges in practically implementing an IPT highway network is determining the sizes of the IPT coils or power pads that are buried in the roadway and mounted on the EV. As the size of these power pads can affect the power transferred, as well as the overall cost of such highways, it is an important design issue for dynamic systems [21]. Moreover, the presence of a variety of EV types (i.e. sedans, SUVs, buses) with differing air-gaps and power requirements also further complicates the problem.

In this paper, an IPT power pad known as the Double-D (DD) is used to transfer power to an EV on the move. This primary pad design was proposed in [22], [23] and consists of two coplanar coils, multiple ferrite strips and an aluminium sheet backing (Fig. 1).

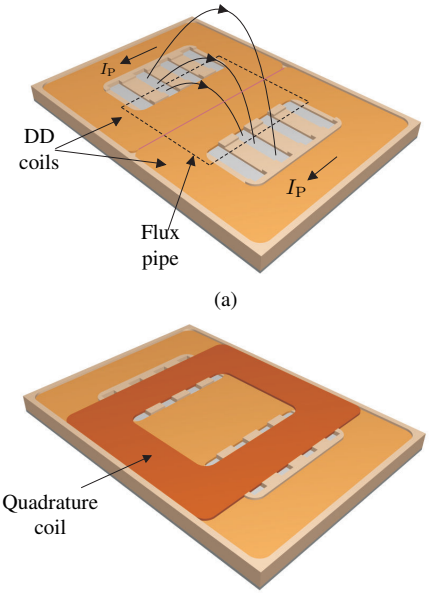

Fig. 1: Double-D (DD) and Double-D Quadrature (DDQ) EV charging pads (a) Energised DD pad showing magnetic flux lines and flux pipe and (b) DDQ secondary pad with spatial quadrature coil.

G. Nagendra is with A.D. Engineering International, Perth, Australia (e-mail: gnagendra555@gmail.com).

G. Covic and J. Boys are currently with the University of Auckland, New Zealand (e-mail: ga.covic@auckland.ac.nz and j.boys@auckland.ac.nz).

Manuscript received June 29, 2016.

2332-7782 (c) 2016 IEEE. Personal use is permitted, but republication/redistribution requires IEEE permission. See http://www.ieee.org/publications_standards/publications/rights/index.html for more information.

This article has been accepted for publication in a future issue of this journal, but has not been fully edited. Content may change prior to final publication. Citation information: DOI 10.1109/TTE.2017.2666554, IEEE Transactions on Transportation Electrification

When the two coils are energised with an AC current (I_{P}), a changing magnetic field is created within the air-gap and thus allows power to be transferred. The ferrite strips form a flux pipe and help to channel the flux within the air-gap thereby improving the coupling and power transfer to a secondary power pad, while the aluminium sheet helps to reduce leakage fields. DD pads can provide significantly higher coupling coefficients than the more traditional Circular pads [24], [25]. Moreover, if a spatial quadrature coil is added to the DD to form a DDQ (Fig. 1), then the power transfer capability can be drastically improved. A typical power transfer profile for the DD-DDQ pad combination is shown in Fig. 2. Here, S_{U} is the uncompensated apparent power on the DDQ and is the product of the induced open circuit voltage (V_{OC}) and short circuit current (I_{SC}).

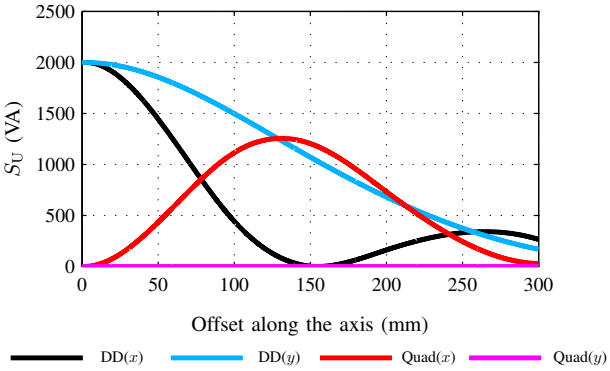

Fig. 2: S_{U} profile for the DD-DDQ pad based EV charging system. Here the traces are named according to the coil and offset direction e.g. DD(x) refers to the S_{U} profile of the DD coil as xos is varied with the x-axis being aligned with the length of the primary pad.

In [23], it was found that the DD-DDQ pad combination could achieve higher coupling and a charging zone more than 5 times larger in terms of coverage area than that of an equivalent Circular pad system. Importantly, as the DD-DDQ combination does not suffer from a null in the power transfer zone (unlike a Circular based system), it is ideally suited for highway applications where a large degree of lateral movement is desired. As such, this paper focusses on pad sizing for DD-DDQ based systems - although it should be noted that the techniques developed can be easily applied to other pad structures.

In [23], a method to size DD pads for EV applications was also presented. While the design methods outlined are very helpful for matched systems, they are also limited in that they specifically focussed on identically sized primary and secondary pad combinations to simplify the problem. In [21], an approach was proposed to size DD pads in stationary 10 kW IPT systems where the primary and secondary pads were different in size. The results from this analysis also showed how pads could be designed for differing vehicle classes (i.e sedans and SUVs) as well as charging locations (e.g garages, car-parks and roadways). Table I summarizes the dimensions of the primary and secondary pads used in [21]. Here, "Pri" or "Sec" refer to either the primary or secondary pad respectively, while the two numbers refer to the length and width of the pad in mm. For example, $\mathrm{Pri\_255\_280}$ refers to a primary pad that is 255 mm long and 280 mm wide.

TABLE I: Proposed pad sizes.

Primary pads	Secondary pads
$\mathrm{Pri\_255\_280}$	$\mathrm{Sec\_280\_325}$
$\mathrm{Pri\_395\_390}$	$\mathrm{Sec\_370\_410}$
$\mathrm{Pri\_510\_475}$	$\mathrm{Sec\_465\_495}$
$\mathrm{Pri\_630\_620}$	$\mathrm{Sec\_560\_580}$
$\mathrm{Pri\_745\_705}$	$\mathrm{Sec\_745\_690}$
$\mathrm{Pri\_745\_825}$	$\mathrm{Sec\_835\_800}$
$\mathrm{Pri\_865\_910}$	$\mathrm{Sec\_930\_885}$
$\mathrm{Pri\_980\_995}$	$\mathrm{Sec\_1025\_1030}$

This paper aims to further develop the pad sizing analysis detailed in [21], and extend it to dynamic IPT EV highways. As such, this paper expands upon the concepts presented in [21], to include EV charging of vehicles (sedans and SUVs) as they move. Consequently, this paper studies the power transfer profiles when multiple IPT primary pads (Table I) are simultaneously energised and the effect that this has on the overall power transfer to the EV. In Section II of this paper, the proposed IPT highway is presented. Section III explores the cross coupling between adjacent IPT primary pads and the effect this has on the power transfer profile. Section IV proposes a mathematical model for power transfer on the highway while Sections V and VI use this model to predict power transfer with multiple primary pads. Sections VII to IX outline a practical design example that highlights how the given analysis can be used to select IPT pad sizes for dynamic highway applications. Finally, Section X summarizes the key conclusions of the research presented.

II. Proposed IPT Highway

A lumped IPT highway could be represented by Fig. 3(a). In this illustration, IPT primary pads are buried under the road along the direction of EV travel with secondary pads mounted to the underside of the EV chassis.

As the EV travels along the highway, the primary pads are sequentially energised when the EV secondary pad has sufficient coupling with the respective primary pad. For example when the EV is directly above a buried primary pad, as shown in Fig. 3(b), then only this primary pad is energised as it has the greatest coupling to the EV pad. However, when the EV is in between two primary pads, as shown in Fig. 3(c), then both primary pads may be energised to increase power transfer even though the individual coupling between each primary pad and the EV may be reduced due to the offset. Using this approach, a reasonably constant wave of power may be transferred to the EV as it travels along the highway. Moreover, this approach can easily be extended to allow charging of multiple vehicles on the highway simultaneously.

In a lumped DD and DDQ based IPT highway, there are two main ways in which the pads may be orientated along the highway. In Fig. 4(a), the DD primary and secondary pads are

2332-7782 (c) 2016 IEEE. Personal use is permitted, but republication/redistribution requires IEEE permission. See http://www.ieee.org/publications_standards/publications/rights/index.html for more information.

This article has been accepted for publication in a future issue of this journal, but has not been fully edited. Content may change prior to final publication. Citation information: DOI 10.1109/TTE.2017.2666554, IEEE Transactions on Transportation Electrification

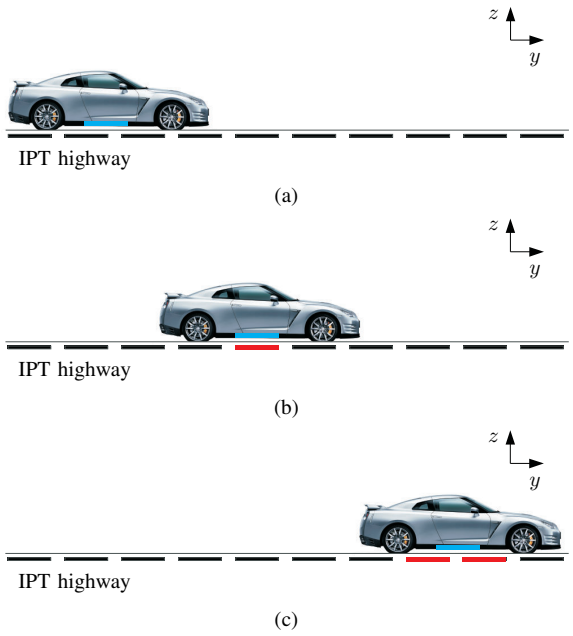

Fig. 3: (a) IPT EV highway with primary pads shown in black and EV mounted secondary pad shown in blue. (b) Highway showing energised primary pad in red when the EV is directly above one primary pad. (c) Highway showing energised primary pads in red when the EV is above 2 primary pads.

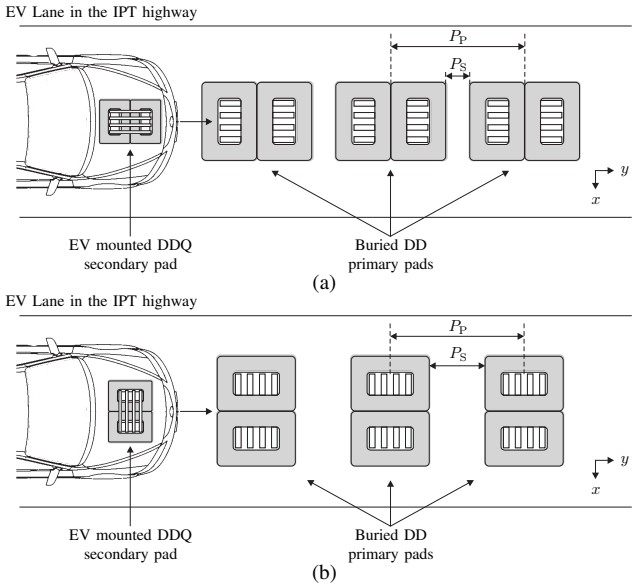

Fig. 4: Possible pad orientations in the proposed IPT EV highway with (a) pads arranged parallel to the direction of EV travel and (b) pads arranged perpendicular to the direction of EV travel.

orientated so that the DD coils are parallel to the direction of EV travel while in Fig. 4(b), the pads are orientated so that the DD coils are perpendicular to the direction of EV travel. In both orientations, the distance between the centres of the primary pads is referred to as the primary pad pitch (P_{P}), and the spacing between the primary pad cases is referred to as the primary pad spacing (P_{S}). Both possible orientations offer certain benefits for dynamic EV powering applications.

The main advantage offered by the orientation shown in Fig. 4(a) is the possible reduction in general public exposure to unwanted or potentially harmful electromagnetic fields. In general, the length of a DD pad is usually larger than its width. This is mainly due to the fact that the length of the pad, or the distance between the poles, has the largest impact on the flux path height or the possible operational air-gap [23]. On the other hand the width of the pads is usually varied to modify the shape of the power transfer profile or increase the power transfer as necessary. Hence by placing these rectangular primary pads parallel to the direction of travel or parallel to the EV body, the aluminium or steel EV chassis can significantly help to shield the general public from the electromagnetic fields generated when the primary pad is energised. In dynamic EV applications, however, human exposure to magnetic fields is not of prime concern as it is very unlikely that the general public will be in close proximity to the EV when it is travelling along the highway at speeds close to 100 km/hr. Moreover, by using a lumped IPT pad system, the average generated leakage $\boldsymbol{B}$ is already minimised as the pads are only energised when the EV chassis is partially shielding the pads.

By using the orientation given in Fig. 4(b), a charging system can be designed that is more tolerant of the average driver's ability. In reality, it will be impractical for an average driver travelling at 100 km/hr to manually align their EV as it travels along the centre of the highway and keep the primary and secondary pads close to perfectly aligned. Hence any IPT highway system has to be tolerant to relatively large misalignments (approx. $\pm$300 mm) on the x-axis direction and still transfer the required power to the EV.

Typically for the DD-DDQ pad system, the drop in power is far greater when the secondary pad is offset along the y-axis compared to offsets along the x-axis. This can be seen in the S_{U} profiles given in Fig. 2. Due to the additive contribution of the Quadrature coil, the S_{U} profile for offsets along the x-axis does not drop in magnitude as much as it does along the y-axis. Consequently by placing the pads as shown in Fig. 4(b), the tolerance of the system to large misalignment along the x axis due to driver ability can be greatly increased. Moreover, the power transfer when the EV is offset along the y-axis can be increased if two adjacent primary pads are energised simultaneously as discussed earlier. As a result, in this paper, the orientation given in Fig. 4(b) is the design selected for further evaluation of an IPT highway. Moreover, it is assumed that the primary pads are sequentially energised by primary power supplies near the roadway. One such layout is outlined in Fig. 7 of [15] with separately energised pads. There are several alternative methods of energising the pads and a full discussion of this is outside the scope of the paper. This paper mainly focuses on the sizing of known pads that can be used for an IPT highway, while future papers will focus on how these selected pad sizes can be suitably energised by primary power supplies on a highway.

Of course other variations in the possible pad orientations exist. These include possibly staggering the pads, similar to the approach used in brick laying, or even skewing the pads by an angle so that the power transfer profiles can be altered. However exploring such possibilities is unfortunately out of

2332-7782 (c) 2016 IEEE. Personal use is permitted, but republication/redistribution requires IEEE permission. See http://www.ieee.org/publications_standards/publications/rights/index.html for more information.

This article has been accepted for publication in a future issue of this journal, but has not been fully edited. Content may change prior to final publication. Citation information: DOI 10.1109/TTE.2017.2666554, IEEE Transactions on Transportation Electrification

the scope of this paper but could be investigated in the future.

Budhia first introduced the lumped DD-DDQ based IPT EV highway in [26], and investigated the achievable power transfer profile when multiple primary pads along the highway are energised simultaneously. In this investigation, a single DD and DDQ pad size was used and the resulting power transfer profiles obtainable, by energising multiple combinations of primary pads, were simulated and experimentally verified. In addition, the spacing between adjacent primary pads (P_{S}), or pad pitch (P_{P}), was also varied and the effects on the power transfer profiles were investigated. However, a full investigation of the effects of the size of the IPT pads on the power transfer profile was not carried out as it was beyond the scope of his research. For the same reason, the spacing between adjacent primary pads was not optimised to minimise the number of pads while still ensuring the desired power transfer levels. In the following sections, these key topics are explored to allow for the practical design of IPT highways to power multiple EV classes.

III. Cross Coupling between Adjacent Primary Pads

One of the important considerations when designing an IPT highway is the level of magnetic cross coupling between adjacent primary pads along the highway. If the level of magnetic coupling between the pads is high, then when a primary pad is energised with a current (I_{P}), a large voltage will be induced in the adjacent primary pads. This could cause a large unwanted current to inadvertently flow in these pads generating loss and stray electromagnetic fields. This large induced current will also reflect a load back on the primary power supply driving the desired primary pad, and if both pads are being energised, could cause energy to be fed from one pad to another. This extra loading of the power supply or cycling of energy between pads should be minimised as it has the effect of increasing system loss and the required component ratings, whilst not increasing the power transfer to the EV. To investigate the mutual coupling between pads, a DD primary pad was energised with a current I_{P} of 26 A at 20 kHz and the S_{U} induced in an adjacent DD primary pad was measured experimentally. The spacing between the DD primary pad cases or P_{S} was then varied and the resulting profile is shown in Fig. 5.

It can be seen that the S_{U} induced in a primary pad when the adjacent primary pad is energised is quite low. If the pads are placed so that the separation between pads is 0 mm, the S_{U} induced is only 30 VA in comparison with the approximately 12 kVA generated by the pad. Consequently the coupling or k between these adjacent primary pads is only around 5%, and falls rapidly as the spacing between the pads is increased. Hence if the pads are placed more than 50 mm apart in the IPT highway, the level of magnetic cross coupling between adjacent primary pads is negligible and can be ignored.

IV. Mathematical Modelling of Power Transfer Profiles

In [21], eight approximately square primary DD and secondary DDQ pads ranging in length from 300 - 1000 mm

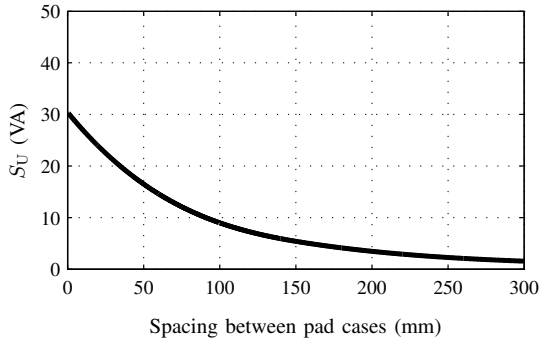

Fig. 5: S_{U} induced in one DD primary pad when the adjacent DD primary pad is energised with no secondary pad present. The S_{U} profile is obtained experimentally by varying the spacing between the primary pad cases (P_{S}) in the laboratory scale system.

were explored for EV charging applications. To predict the performance of these pads, a Finite Element Method (FEM) based model was constructed in JMAG Studio. This software package has been used extensively to analyse IPT power pads, and the resulting simulations have also been validated experimentally in numerous publications [22]–[25].

In these JMAG simulations, the pads were simulated for horizontal offsets along the y-axis ranging from 0 mm to 300 mm in 50 mm intervals. For the purposes of stationary charging such a range of offsets are very practical as most drivers can align their vehicle to the primary pad within such tolerances. However in an IPT highway in which the EV is moving along the y-axis, a larger range of offsets will be encountered. One possible way to obtain information about the expected performance is to re-run the simulations for larger horizontal offsets. But these simulations would take excessive amounts of time to complete and hence this method is not practical. Another method of predicting the performance of the pads for larger offsets is to develop a mathematical model or a set of equations that describe the performance of the pads. Such equations could describe, for example, the V_{OC} profiles for a pad and could predict V_{OC} for offsets greater than 300 mm.

In essence, a window function is required to model the performance of the pads for the required offsets. In this paper, a Gaussian model based function is used to predict the desired IPT power transfer profiles. In this case, the Gaussian function is a simple means of modelling the approximately bell-shaped IPT power transfer profiles, and does not refer to a statistical or probabilistic distribution. Of course, alternative window functions based on Hanning or raised cosines could be used with slight modifications to the general approach presented here [27].

This Gaussian model would have the generalised form of (1) with its parameters being explained by Table II.

$$\zeta = a \cdot e^{-\left(\frac{yos-b}{c}\right)^2} \tag{1}$$

2332-7782 (c) 2016 IEEE. Personal use is permitted, but republication/redistribution requires IEEE permission. See http://www.ieee.org/publications_standards/publications/rights/index.html for more information.

This article has been accepted for publication in a future issue of this journal, but has not been fully edited. Content may change prior to final publication. Citation information: DOI 10.1109/TTE.2017.2666554, IEEE Transactions on Transportation Electrification

TABLE II: Gaussian model parameters.

Parameter	Description
ζ	Quantity to be modelled (e.g. $V_{\mathrm{OC-DD}}$, $V_{\mathrm{OC-QUAD}}$, $I_{\mathrm{SC-DD}}$, or $I_{\mathrm{SC-QUAD}}$)
yos	Offset along the y-axis
a	Amplitude or peak value of the distribution
b	Location of the peak along the y-axis
c	Related to the width of the peak in the distribution

To obtain the a, b and c parameters for the distributions, the data points obtained from the JMAG Studio simulations for y-offsets ranging from 0 mm to 300 mm may be used in conjunction with a curve fitting algorithm. Such fitting algorithms are readily available in MATLAB and can be applied to determine the value of these parameters by minimising the errors between the fit model and the simulated data points. As an example, Fig. 6 shows the simulated V_{OC} data points and the corresponding fitted Gaussian model ($a = 100.9$ V, $b = 0$ mm, and $c = 280.6$ mm). It is clear that the Gaussian model fits these data points quite well within the range of -300 mm to 300 mm. Moreover, the model shows close agreement with experimental results within the range of -300 mm to 300 mm. For offsets greater than this, the Gaussian model and experimental results differ slightly by around 5 V. However, as this is only around 5% of the peak value of 100.9 V, such differences are negligible and can thus be neglected. Similarly, the curve fitting algorithm can easily be used to fit Gaussian distributions to the other results obtained from the simulations such as M_{DD}, I_{SC} and S_{U}. It should be noted that the a, b and c parameters obtained only correspond to a particular operating condition. If for example these conditions are altered, e.g. the air-gap (zos) is changed, then new parameters would have to be found to fit the modified system. However, the use of these parameters and Gaussian model allows for an analytical description of the power transfer profiles to be developed, and hence will be useful when theoretically predicting the performance of multiple pads part of the IPT highway.

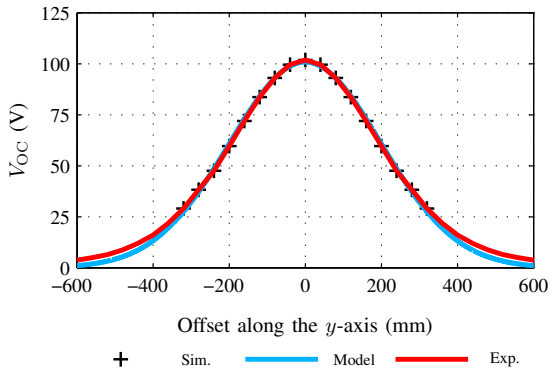

Fig. 6: Typical V_{OC} profile used for modelling of power transfer profiles. The figure shows the simulated data points, the predicted output from the Gaussian model and the experimental results.

V. Power Transfer Profiles with Two Energised Primary Pads

To analyse the performance when multiple primary pads are energised simultaneously, first consider a system consisting of only two primary pads. In this system, the two primary pads are spaced apart and energised with currents given by

$$I_{\mathrm{P1}} = \hat{I}_{\mathrm{P1}} \cdot \cos(\omega t) \tag{2}$$

$$I_{\mathrm{P2}} = \hat{I}_{\mathrm{P2}} \cdot \cos(\omega t + \theta) \tag{3}$$

where I_{P1} and I_{P2} are the currents used to energise primary pad 1 and 2 respectively, and $\hat{}$ represents the peak quantity. It should be noted that this assumes that the system has reached steady state before the EV has entered the optimum charging zone. Practically, the time taken to reach steady state is highly dependent on the circuit parameters and control algorithm. For example, it has been experimentally demonstrated that the charging current to an EV battery could reach steady state in less than 2.5 ms [28]. An EV travelling at 100 km/hr would travel approximately 69 mm in this time. However, in order to ensure that steady state operation has been reached (and hence that the phasor analysis is valid), the EV must be detected 2.5 ms before it enters the optimum charging zone for the IPT pads. This can be easily done by adjusting the sensors that are used to detect the presence of the EV and energising the primary pads accordingly. This means that the primary pads will be energised prior to the EV arrival, and the system can reach steady state before the EV actually enters the optimum charging zone. Moreover, it was shown in [29] that with proper controller design these pads can be energised and ready to transfer power within 0.3 ms. If an EV is travelling at 100 km/hr, then it would move approximately 8 mm in this time. Therefore at these speeds, providing the detection is achieved accurately (which has been discussed in [19]), the energization of the primary pad need occur only a few cm ahead of the optimum coupling zone.

Consequently, the V_{OC} and I_{SC} profiles induced in the secondary pad are simply a combination of the contributions from both primary pads taking the phase difference (θ) between I_{P1} and I_{P2} into account. For example, the I_{SC} generated by energising each primary pad separately can be given by (4) and (5). Here, I_{SC1} is the short circuit current when primary pad 1 is separately energised, and I_{SC2} is the short circuit current when primary pad 2 is separately energised. The resultant I_{SC} or I_{SCR} is the sum of these currents and is shown in (6).

$$I_{\mathrm{SC1}} = \hat{I}_{\mathrm{SC1}} \cdot \cos(\omega t) \tag{4}$$

$$I_{\mathrm{SC2}} = \hat{I}_{\mathrm{SC2}} \cdot \cos(\omega t + \theta) \tag{5}$$

$$I_{\mathrm{SCR}} = \hat{I}_{\mathrm{SC1}} \cdot \cos(\omega t) + \hat{I}_{\mathrm{SC2}} \cdot \cos(\omega t + \theta) \tag{6}$$

It should be noted that these currents or profiles can only be summed as the cross coupling between adjacent primary pads is negligible when they are spaced slightly apart. As a result, the primary pads have minimal interaction with one another and can be assumed to operate independently. The relations can also be expressed using phasor representations:

2332-7782 (c) 2016 IEEE. Personal use is permitted, but republication/redistribution requires IEEE permission. See http://www.ieee.org/publications_standards/publications/rights/index.html for more information.

This article has been accepted for publication in a future issue of this journal, but has not been fully edited. Content may change prior to final publication. Citation information: DOI 10.1109/TTE.2017.2666554, IEEE Transactions on Transportation Electrification

$$\boldsymbol{I}_{\mathrm{SC1}} = \hat{I}_{\mathrm{SC1}}\angle 0 \; = \hat{I}_{\mathrm{SC1}}(\cos 0 + j \sin 0) \tag{7}$$

$$\boldsymbol{I}_{\mathrm{SC2}} = \hat{I}_{\mathrm{SC2}}\angle \theta \; = \hat{I}_{\mathrm{SC2}}(\cos \theta + j \sin \theta) \tag{8}$$

$$\boldsymbol{I}_{\mathrm{SCR}} = \hat{I}_{\mathrm{SCR}}\angle \psi = \hat{I}_{\mathrm{SCR}}(\cos \psi + j \sin \psi) \tag{9}$$

The phasor representations of the I_{SC} generated by each primary pad can also be understood graphically through the use of a phasor diagram shown in Fig. 7.

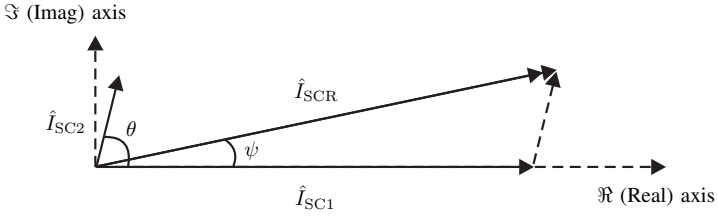

Fig. 7: Phasor diagram showing $\boldsymbol{I}_{\mathrm{SC1}}$, $\boldsymbol{I}_{\mathrm{SC2}}$, and $\boldsymbol{I}_{\mathrm{SCR}}$ phasors.

From the phasor diagram, it is evident that if the cosine rule is applied, the $\hat{I}_{\mathrm{SCR}}$ magnitude can be given by

$$(\hat{I}_{\mathrm{SCR}})^2 = (\hat{I}_{\mathrm{SC1}})^2 + (\hat{I}_{\mathrm{SC2}})^2 - 2\hat{I}_{\mathrm{SC1}}\hat{I}_{\mathrm{SC2}} \cdot \cos(\pi - \theta) \tag{10}$$

$$\hat{I}_{\mathrm{SCR}} = \sqrt{(\hat{I}_{\mathrm{SC1}})^2 + (\hat{I}_{\mathrm{SC2}})^2 + 2\hat{I}_{\mathrm{SC1}}\hat{I}_{\mathrm{SC2}} \cdot \cos\theta} \tag{11}$$

By summing the projections of $\boldsymbol{I}_{\mathrm{SC1}}$ and $\boldsymbol{I}_{\mathrm{SC2}}$ on the $\Re$ axis and equating this to the projection of $\boldsymbol{I}_{\mathrm{SCR}}$ on the $\Re$ axis, the phase (ψ) of $\boldsymbol{I}_{\mathrm{SCR}}$ with respect to I_{P1} is

$$\psi = \begin{cases} \arccos\left(\dfrac{\hat{I}_{\mathrm{SC1}} + \hat{I}_{\mathrm{SC2}}\cos\theta}{\hat{I}_{\mathrm{SCR}}}\right) & \text{if } 0 \le \theta \le \pi \\ -\arccos\left(\dfrac{\hat{I}_{\mathrm{SC1}} + \hat{I}_{\mathrm{SC2}}\cos\theta}{\hat{I}_{\mathrm{SCR}}}\right) & \text{if } \pi < \theta < 2\pi \end{cases} \tag{12}$$

To validate this theoretical analysis, the predicted $\boldsymbol{I}_{\mathrm{SCR}}$ is compared to simulated $\boldsymbol{I}_{\mathrm{SCR}}$ results obtained from a JMAG Studio FEM model of the two primary pad system. In this simulation model, the two DD primary pads are placed with a primary pad pitch (P_{P}) of 600 mm and are simultaneously energised with 25 A RMS at a frequency of 40 kHz. The secondary pad is then placed in the middle of these two primary pads, so that $xos = 0$ mm and $yos = 300$ mm, with an air-gap of 100 mm. With this setup, the corresponding I_{SC} when each primary pad is energised separately gives $\hat{I}_{\mathrm{SC1}} = 2.6658$ A and $\hat{I}_{\mathrm{SC2}} = 2.6661$ A. The phase difference (θ) between I_{P1} and I_{P2} is then varied from 0° to 360° and the expected $\boldsymbol{I}_{\mathrm{SCR}}$ obtained from the FEM model is shown in Fig. 8. The theoretically predicted $\boldsymbol{I}_{\mathrm{SCR}}$, using (11) and (12), shows very close agreement to the simulated results. As a result, the analysis can be used to model $\boldsymbol{I}_{\mathrm{SCR}}$ and reliably predict the performance when multiple primary pads are simultaneously energised.

When designing an IPT highway, maximising I_{SCR} (6) and consequently power transfer is of prime concern. This can be

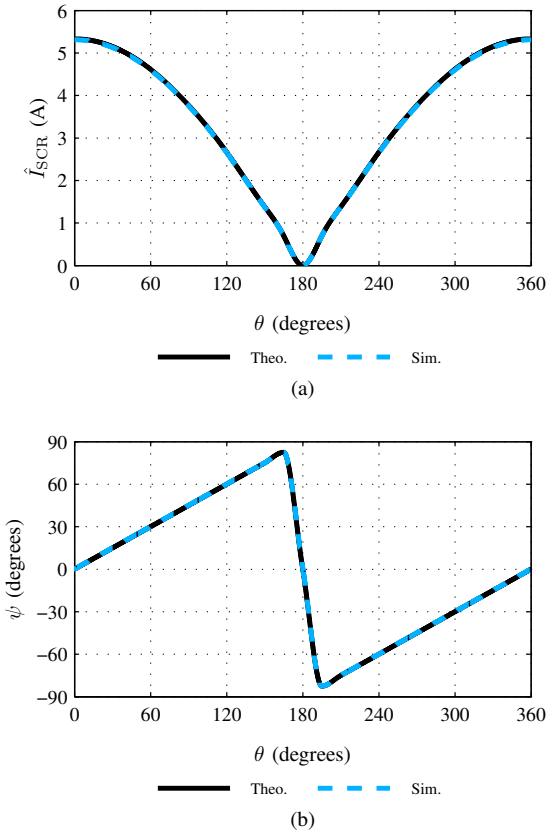

Fig. 8: Theoretical and simulated (a) $\hat{I}_{\mathrm{SCR}}$ and (b) ψ for a two primary pad system as θ is varied.

done by simply maximising the projection of $\boldsymbol{I}_{\mathrm{SCR}}$ on the $\Re$ axis. As this projection is equivalent to $\hat{I}_{\mathrm{SCR}}\cos\psi$, the maximum is achieved when $\hat{I}_{\mathrm{SCR}}$ and $\cos\psi$ are maximised. From Fig. 8, it is evident that this condition is reached and I_{SCR} is maximised when the primary currents are in phase or when $\theta = 0° = 0$ rads. This is intuitive as it represents the case where the angle between $\boldsymbol{I}_{\mathrm{SC1}}$ and $\boldsymbol{I}_{\mathrm{SC2}}$ is zero and consequently the magnitude of the $\hat{I}_{\mathrm{SCR}}$ given in (11) is maximum. Similarly, a phasor diagram can also be used to predict the resultant $\hat{V}_{\mathrm{OC}}$ from energising both primary pads. However, as I_{SC} mainly controls the power transfer for parallel compensated secondaries, the I_{SCR} profiles are the main focus for the rest of the analysis. Importantly, when $\theta = 0$ rads then

$$\hat{I}_{\mathrm{SCR}} = \hat{I}_{\mathrm{SC1}} + \hat{I}_{\mathrm{SC2}} \tag{13}$$

$$\hat{V}_{\mathrm{OCR}} = \hat{V}_{\mathrm{OC1}} + \hat{V}_{\mathrm{OC2}} \tag{14}$$

It is also interesting to note that even if θ varies slightly (e.g. $\pm 15°$), there is a negligible drop in $\hat{I}_{\mathrm{SCR}}$ and hence I_{SCR}. This result shows that appreciable power transfer to the secondary can still be achieved even if the primary pad currents are not perfectly in phase.

VI. Power Transfer Profiles with Multiple Energised Primary Pads

In the case of an IPT highway where multiple primary pads may be simultaneously energised in phase to maximise power

2332-7782 (c) 2016 IEEE. Personal use is permitted, but republication/redistribution requires IEEE permission. See http://www.ieee.org/publications_standards/publications/rights/index.html for more information.

This article has been accepted for publication in a future issue of this journal, but has not been fully edited. Content may change prior to final publication. Citation information: DOI 10.1109/TTE.2017.2666554, IEEE Transactions on Transportation Electrification

transfer to the EV, the resulting I_{SCR} and V_{OCR} profiles are simply the sum of the contributions from each of the primary pads. As energising adjacent primary pads can help increase the power transfer that is possible, it should be evident that three primary pads are sufficient to model the power transfer along the highway. Of course, while only three primary pads may be energised at one time, multiple primary pads are involved in transferring power to the EV as it moves along the highway.

Applying the approach outlined in Section IV, a Gaussian model can be developed to mathematically describe the I_{SC} profiles generated by energising each primary pad independently. As each primary pad is identical in size, the a and c parameters in the Gaussian model are constant with the b parameter used to shift the distribution along the y-axis accordingly. With three primary pads separated by the pad pitch (P_{P}), the Gaussian distributions are given by

$$I_{\mathrm{SC1}} = a \cdot e^{-\left(\frac{yos}{c}\right)^2} \tag{15}$$

$$I_{\mathrm{SC2}} = a \cdot e^{-\left(\frac{yos - P_{\mathrm{P}}}{c}\right)^2} \tag{16}$$

$$I_{\mathrm{SC3}} = a \cdot e^{-\left(\frac{yos - 2P_{\mathrm{P}}}{c}\right)^2} \tag{17}$$

The I_{SCR} profile is then the sum of these individual I_{SC} profiles and is

$$I_{\mathrm{SCR}} = I_{\mathrm{SC1}} + I_{\mathrm{SC2}} + I_{\mathrm{SC3}} \tag{18}$$

$$I_{\mathrm{SCR}} = a \cdot e^{-\left(\frac{yos}{c}\right)^2} + a \cdot e^{-\left(\frac{yos - P_{\mathrm{P}}}{c}\right)^2} + a \cdot e^{-\left(\frac{yos - 2P_{\mathrm{P}}}{c}\right)^2} \tag{19}$$

The maximum I_{SCR} occurs, intuitively, directly above the second primary pad as I_{SCR} has the maximum contributions from all three primary pads. The maximum I_{SCR} is then

$$I_{\mathrm{SCR-MAX}} = I_{\mathrm{SCR}}(yos = P_{\mathrm{P}}) = a + 2a \cdot e^{-\left(\frac{P_{\mathrm{P}}}{c}\right)^2} \tag{20}$$

The minimum I_{SCR} occurs between the pads where $yos = P_{\mathrm{P}}/2$ or $yos = 3P_{\mathrm{P}}/2$. Hence the minimum I_{SCR}, the average I_{SCR} and the corresponding variation in I_{SCR} ($\delta I_{\mathrm{SCR}} = I_{\mathrm{SCR-MAX}} - I_{\mathrm{SCR-MIN}}$) can be given by

$$I_{\mathrm{SCR-MIN}} = 2a \cdot e^{-\left(\frac{P_{\mathrm{P}}}{2c}\right)^2} + a \cdot e^{-\left(\frac{3P_{\mathrm{P}}}{2c}\right)^2} \tag{21}$$

$$I_{\mathrm{SCR-AVG}} = \frac{a}{2} + a \cdot e^{-\left(\frac{P_{\mathrm{P}}}{c}\right)^2} + a \cdot e^{-\left(\frac{P_{\mathrm{P}}}{2c}\right)^2} + \frac{a}{2} \cdot e^{-\left(\frac{3P_{\mathrm{P}}}{2c}\right)^2} \tag{22}$$

$$\delta I_{\mathrm{SCR}} = a + 2a \cdot e^{-\left(\frac{P_{\mathrm{P}}}{c}\right)^2} - 2a \cdot e^{-\left(\frac{P_{\mathrm{P}}}{2c}\right)^2} - a \cdot e^{-\left(\frac{3P_{\mathrm{P}}}{2c}\right)^2} \tag{23}$$

Using the Gaussian models developed here it is also possible to predict the I_{SCR} profile for a three pad highway. To validate the model, the predicted profiles are compared with experimental results obtained from a prototype laboratory scale IPT highway that was presented in [26]. In this laboratory setup, three DD primary pads were spaced apart with a pad pitch (P_{P}) of 525 mm where the pad pitch represents the distance between the centres of the primary pads. The primary pads were each driven in phase ($\theta = 0$) with 11.5 A at 20 kHz with each individual primary power supply being synchronised by a master controller as described in [30]. A DDQ secondary pad was then moved over the prototype highway along the y-axis, with $xos = 0$ mm, and the resulting I_{SC} profiles are given in Fig. 9. The figure shows the positions of each of the three primary pads (Pads 1, 2, and 3) located at $yos = 0$ mm, $yos = P_{\mathrm{P}}$ mm, and $yos = 2P_{\mathrm{P}}$ mm respectively. The corresponding I_{SC} profiles as each pad is energised independently are also shown clearly.

From these profiles, the corresponding Gaussian models can be created with $a = 5.1808$ A, $c = 282.9540$ mm and $P_{\mathrm{P}} = 525$ mm. Using the developed models and the analysis presented earlier, the theoretical I_{SCR} profile can be obtained and is also shown in Fig. 9. It is evident that this predicted profile shows very close agreement with the experimental I_{SCR} profile obtained from the laboratory prototype system. Very importantly, the I_{SCR} profiles show that the I_{SC} used to charge an EV can be significantly increased by energising multiple primary pads in the highway.

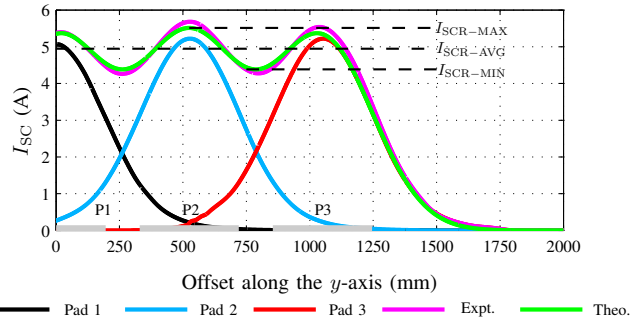

Fig. 9: IPT highway showing the three primary pads (P1, P2, and P3) and the corresponding I_{SC} profiles as each pad is energised independently. In addition, the theoretically predicted and experimentally measured I_{SCR} profiles are also shown. All experimental results were kindly provided by Dr. Mickel Budhia.

With the Gaussian models of the I_{SC} profiles, it is also possible to predict $I_{\mathrm{SCR-MAX}}$, $I_{\mathrm{SCR-MIN}}$, $I_{\mathrm{SCR-AVG}}$, and δI_{SCR} for the laboratory system. The theoretically predicted results (Table III) show close agreement with the experimental results.

TABLE III: Theoretical predictions and experimental measurements of $I_{\mathrm{SCR-MAX}}$, $I_{\mathrm{SCR-MIN}}$, $I_{\mathrm{SCR-AVG}}$, and δI_{SCR}.

Variable	Theoretical	Experimental	Error
$I_{\mathrm{SCR-MAX}}$ (A)	5.5122	5.68	-2.95%
$I_{\mathrm{SCR-MIN}}$ (A)	4.3840	4.26	$+2.91\%$
$I_{\mathrm{SCR-AVG}}$ (A)	4.9481	4.97	-0.44%
δI_{SCR} (A)	1.1282	1.20	-5.98%

By adding more primary pads and extending the IPT highway, it is possible to see how power can be transferred to the

2332-7782 (c) 2016 IEEE. Personal use is permitted, but republication/redistribution requires IEEE permission. See http://www.ieee.org/publications_standards/publications/rights/index.html for more information.

This article has been accepted for publication in a future issue of this journal, but has not been fully edited. Content may change prior to final publication. Citation information: DOI 10.1109/TTE.2017.2666554, IEEE Transactions on Transportation Electrification

EV. Fig. 10 shows the I_{SCR} profile if the laboratory setup is extended so that a 5 m long highway can be considered. The corresponding sequencing or energising order of the primary pads that will be necessary to maintain the I_{SCR} profile is also highlighted. Of course if the approach here is implemented, the length of the highway can be increased as necessary.

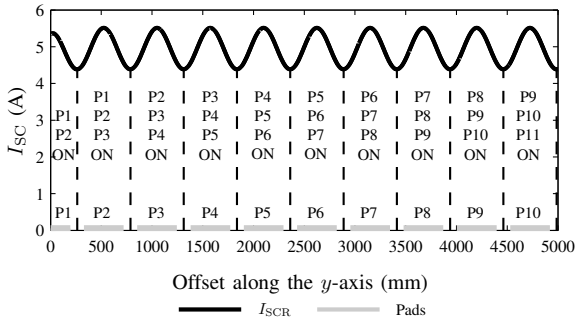

Fig. 10: Theoretical I_{SCR} profile when a 5 m long IPT highway is considered. The necessary sequencing order of the primary pads is also shown.

It should be noted that the analysis presented in this paper has largely ignored the impact of the car-body on the power transfer profiles. This was done as modelling and designing a system while taking into account this metallic car-body is quite difficult. As the analysis presented in this paper uses 11648 simulations [21], it is easy to see that adding the effects of the car chassis will dramatically increase the simulation times and the complexity of the presented mathematical analysis; although with appropriate aluminium shielding means extending out behind the vehicle pad to protect the steel chassis from inadvertent stray fields, the coupling profiles should not change considerably. Moreover, as this paper is mainly focused on providing a valid starting solution to the pad sizing problem, it is reasonable to omit the effects of the car-body initially so that a good starting solution can be obtained. Once this is done, designers can then consider the effects of the car chassis and further optimise the design to better suit the requirements.

VII. Design Example Requirements

With the presented analysis and results for an IPT highway, it is possible to select pad sizes for dynamic IPT highways. A design example is proposed here to demonstrate the approach, and is essentially an extension of the stationary charging design example presented in [21]. In this design example, the same secondary pads proposed in [21] for the sedan and SUV EV classes have to be used. This is to allow the EVs to be charged in both stationary charging locations, such as the garage, as well as dynamically along an IPT highway without needing to change the secondary pad fitted to the EV. It should also be noted that as a short-hand, the pads are denoted on their type and dimensions; for example, $\mathrm{Sec\_465\_495}$ is a secondary DDQ pad with a length of 465 mm and a width of 495 mm.

In addition, it is assumed that the secondary pads are not lowered for charging as the mechanical apparatus required to protect the pads from damage when the EV is travelling at high speeds could be costly. Consequently operational air-gaps (zos) for both the sedan and SUV classes when charged in a roadside location, as given in Table IV, were also used for this design example.

In essence this design example focusses on selecting a primary pad size and pad pitch (P_{P}) to be used in an IPT highway. Ideally the chosen primary pads should be as small as possible and have as large a pad pitch as possible to reduce the necessary resources and cost of the highway. With this being said, if P_{P} is very large then the power transfer profile to the EV as it travels will have large fluctuations and may even be discontinuous. Ultimately, a compromise is necessary to ensure that the primary pads are able to deliver the desired P_{O} levels to both the sedans and SUVs while being cost effective. For this example, a peak power demand of 10 kW is set to power the EV as it travels along the highway. A secondary power flow controller, similar to the one shown in Fig. 11, is then used to regulate this power transfer to the EV [21], [31].

Here, the primary power supply driven by either a single or 3 phase mains input (1ϕ or 3ϕ) comprises of a PFC (Power Factor Correction) stage, a diode rectifier, and an inverter. The power supply then energises the parallel compensated primary DD coil (L_{P}) with an AC current I_{P}. This AC primary current induces a voltage in both the DD and Quadrature coils in the DDQ, given by $V_{\mathrm{OC-DD}}$ and $V_{\mathrm{OC-QUAD}}$ respectively. In order to boost power transfer, the secondary coils are each compensated with a capacitor and hence form current source outputs [21]. These current source outputs can then be rectified and regulated using a standard boost regulator with a switching duty cycle (D) to charge the EV battery (V_{O}). In a typical EV, the output of the boost regulator will possibly be connected to a complex Battery Management System (BMS) that controls the charging of the battery banks using sophisticated control

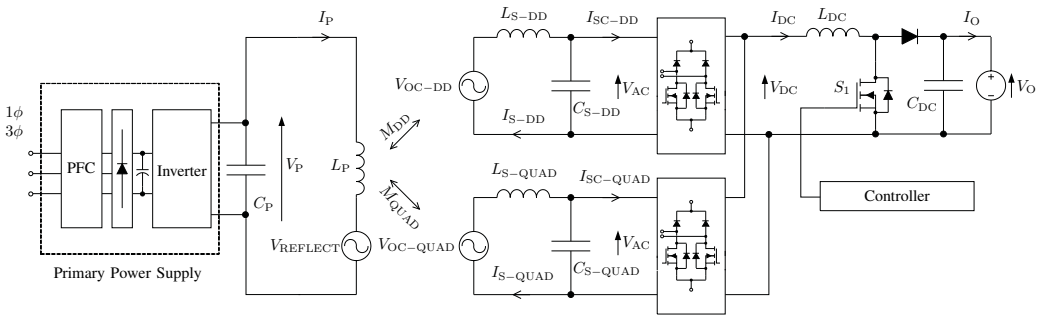

Fig. 11: IPT secondary power flow controller.

2332-7782 (c) 2016 IEEE. Personal use is permitted, but republication/redistribution requires IEEE permission. See http://www.ieee.org/publications_standards/publications/rights/index.html for more information.

This article has been accepted for publication in a future issue of this journal, but has not been fully edited. Content may change prior to final publication. Citation information: DOI 10.1109/TTE.2017.2666554, IEEE Transactions on Transportation Electrification

logic. However, for simplicity of the analysis, the BMS is neglected, and the output of boost regulator is assumed to be a DC voltage source (V_{O}).

It is important to note from [21] that the output power (P_{O}) used to charge the battery is given by

$$P_{\mathrm{O}} = V_{\mathrm{O}} \cdot I_{\mathrm{O}} = \frac{\pi}{2\sqrt{2}} \cdot V_{\mathrm{O}}(1-D)(I_{\mathrm{SC-DD}} + I_{\mathrm{SC-QUAD}}) \tag{24}$$

$$P_{\mathrm{O}} = \frac{\pi}{2\sqrt{2}} \cdot V_{\mathrm{O}}(1-D)(I_{\mathrm{SC-TOTAL}}) \tag{25}$$

With the power demand of 10 kW and a battery voltage of 325 V, the minimum $I_{\mathrm{SC-TOTAL}}$ that can meet this requirement (i.e. $D = 0$) is 28 A. In the IPT highway this $I_{\mathrm{SC-TOTAL}}$ requirement corresponds to an $I_{\mathrm{SCR-MIN}}$ requirement as multiple primary pads will naturally be energised simultaneously in phase. It is evident from Fig. 10, that the I_{SCR} and hence power transferred to the EV varies depending on the position of the EV along the highway. Thus if I_{SCR} is larger than 28 A, the secondary controller ensures that P_{O} is limited to 10 kW by making $D > 0$. If however I_{SCR} falls below 28 A as the EV moves over the highway primary pads, then $D = 0$ and P_{O} falls below 10 kW. Ideally $I_{\mathrm{SCR-MIN}}$ will be 28 A so that a constant 10 kW may be transferred to the EV as it travels. However this will require a reduction in the pad pitch (P_{P}) or an increase in the primary pad sizes so that I_{SCR} is always above the requirement as the EV travels. This will have the effect of increasing the number of pads or the resources used which will inadvertently increase the cost of the IPT highway. As a result, for this example, the power transfer is allowed to drop by a maximum of 25% and correspondingly the $I_{\mathrm{SCR-MIN}}$ is allowed to drop by 25% to 21 A. A summary of the requirements for this design example is shown in Table IV.

TABLE IV: Summary of EV charging parameters and requirements.

Parameter	Value
Secondary pad (Sedan)	Sec_465_495
Secondary pad (SUV)	Sec_930_885
zos (Sedan)	250 mm
zos (SUV)	400 mm
I_{P}	25 A per winding
f	40 kHz
P_{O}	10 kW
V_{O}	325 V DC
Ideal $I_{\mathrm{SCR-MIN}}$	28 A
Allowed $I_{\mathrm{SCR-MIN}}$	21 A

VIII. Design Methodology

The first step in the design process involves extracting the I_{SC} profiles obtained from the JMAG simulations described in [21]. These profiles correspond to the simulation results obtained when each of the eight primary pads are used to power both the sedan and SUV secondary pads for the desired air-gaps given in Table IV.

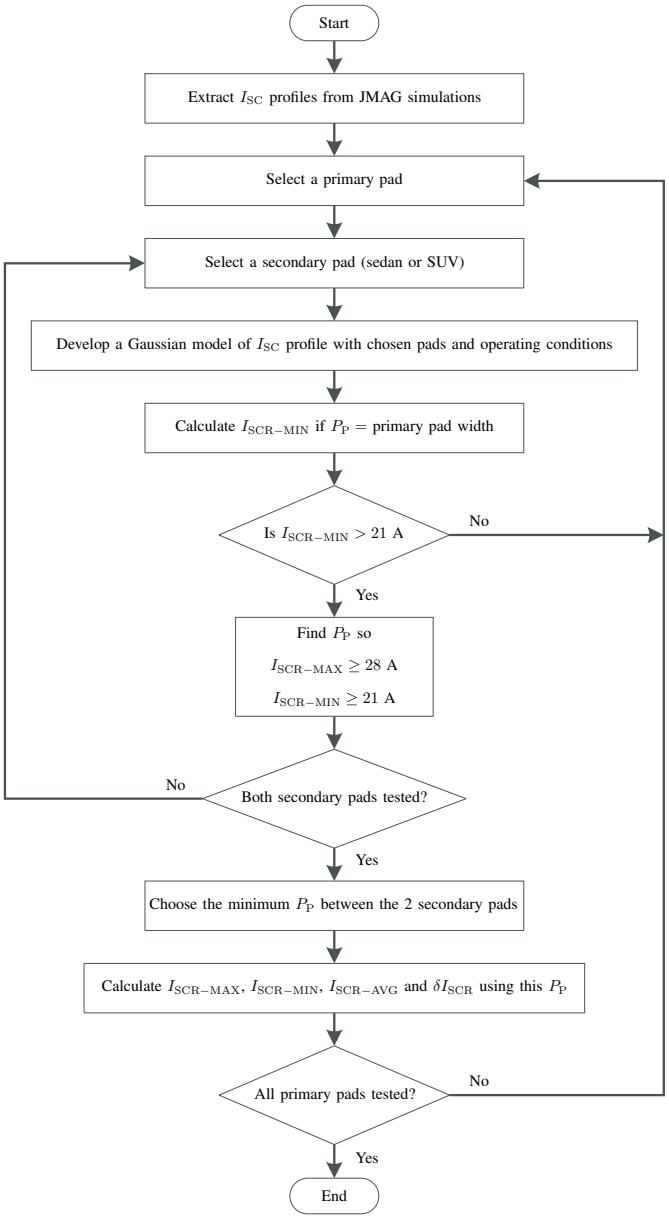

Fig. 12: Pad sizing method for the dynamic EV charging design example.

Following this, one of the eight primary pads and one of the secondary pads used for either the sedan or the SUV charging is chosen for analysis. Using the curve fitting algorithms briefly mentioned earlier in Section IV, a Gaussian model is then developed to approximate the I_{SC} profile of the chosen primary and secondary pads. This algorithm provides the required a and c parameters to accurately model the I_{SC} profile using a Gaussian distribution. Using (21), the $I_{\mathrm{SCR-MIN}}$ is then calculated for the given distribution for the case where the chosen primary pads are placed without spacing between them, or where P_{P} is equal to the width of the primary pad. If $I_{\mathrm{SCR-MIN}}$ is below the 21 A requirement outlined in Table IV, then the chosen primary pad need not be considered further as the pad combination will not be able to meet the requirement if the pad pitch is increased. On the other hand, if $I_{\mathrm{SCR-MIN}} > 21$ A, then a primary pad pitch can be

2332-7782 (c) 2016 IEEE. Personal use is permitted, but republication/redistribution requires IEEE permission. See http://www.ieee.org/publications_standards/publications/rights/index.html for more information.

This article has been accepted for publication in a future issue of this journal, but has not been fully edited. Content may change prior to final publication. Citation information: DOI 10.1109/TTE.2017.2666554, IEEE Transactions on Transportation Electrification

found by numerically solving (20) and (21) for P_{P} so that $I_{\mathrm{SCR-MAX}} \geq 28$ A and $I_{\mathrm{SCR-MIN}} \leq 21$ A. This process is then simply repeated for the other secondary pad. For a particular primary pad, the minimum P_{P} that can meet the requirements for both the sedan and SUV classes is chosen so that the designed highway can simultaneously meet the charging requirements for both EV classes. Using this P_{P}, the corresponding $I_{\mathrm{SCR-MAX}}$, $I_{\mathrm{SCR-MIN}}$, $I_{\mathrm{SCR-AVG}}$ and δI_{SCR} for both the sedan and SUV classes can then be calculated using the Gaussian models and (20)-(23). This entire process is then repeated until all the primary pads are tested. A summary of this proposed method to select the primary pad size and pad pitch for an IPT highway is shown in Fig. 12.

IX. Results

For the proposed design example, the corresponding a and c parameters for the various primary pads and secondary pads are shown in Table V and Table VI. It should be noted, that for this design example, it is assumed that the EV or secondary pad is perfectly aligned along the x-axis (e.g. $xos = 0$ mm) as it travels along the y-axis. This provides a good starting point when designing an IPT highway, and further work or optimisation can look to modifying the highway to ensure the required horizontal tolerance along the x-axis can be met.

As mentioned if P_{P} is equal to the primary pad width, then the various primary pads can be rapidly tested to see if they are likely to meet the requirements should P_{P} be increased. From Table V, it is evident that through this preliminary testing $\mathrm{Pri\_255\_280}$ to $\mathrm{Pri\_630\_620}$ can be removed from consideration as they are unable to meet the $I_{\mathrm{SCR-MIN}}$ requirements for charging of both the sedan and SUV classes.

By numerically solving (20) and (21) to find a value for P_{P} to simultaneously meet the $I_{\mathrm{SCR-MAX}}$ and $I_{\mathrm{SCR-MIN}}$ requirements for both the sedan and SUV classes, a suitable P_{P} value can be determined for IPT highways using varying sized primary pads ($\mathrm{Pri\_745\_705}$ to $\mathrm{Pri\_980\_995}$). The selected primary pad pitches (P_{P}) using these primary pads are given in Table VII. Based on this P_{P}, the key variables can be calculated ((20)-(23)) for the highway.

As highways based on each of these primary pads are capable of meeting the outlined requirements, the selection of a particular primary pad for this design example requires careful consideration. A simple means of comparing the primary pads is by considering the materials or resources used by highways based on these primary pads. The mass of ferrite and length of Litz wire used by each of the primary pads is given in Table VIII.

Using the primary pad pitch given in Table VII, the corresponding number of primary pads necessary per kilometre of highway can be easily calculated. From this the total mass of ferrite and length of Litz necessary per km for each of the highways can also be determined.

From this table it is clear that for this design example, IPT highways using $\mathrm{Pri\_865\_910}$ pads placed with a pad pitch of 1327 mm are ideally suited. Highways based on this primary pad will use the minimum quantity of materials per km and hence can help minimise the overall cost of the IPT highway. Very importantly, such a highway can simultaneously meet the $I_{\mathrm{SCR-MIN}}$ requirements for both the sedan and SUV EV classes with the corresponding predicted I_{SCR} profiles for both EV classes being shown in Fig. 13. Here the output current (I_{O}) is scaled by $\frac{2\sqrt{2}}{\pi}$ to better illustrate its general shape and relationship with I_{SCR}.

TABLE V: Parameters for the generated Gaussian models and the preliminary testing of primary pads $\mathrm{Pri\_255\_280}$ to $\mathrm{Pri\_630\_620}$ with the sedan and SUV secondary pads.

	$\mathrm{Pri\_255\_280}$		$\mathrm{Pri\_395\_390}$		$\mathrm{Pri\_510\_475}$		$\mathrm{Pri\_630\_620}$	
Variable	Sedan	SUV	Sedan	SUV	Sedan	SUV	Sedan	SUV
a (A)	1.81	0.73	7.27	3.17	13.96	6.79	23.60	13.44
c (mm)	319	530	333	530	352	536	399	553
Pad width (mm)	279	279	388	388	473	473	619	619
P_{P} (mm)	279	279	388	388	473	473	619	619
$I_{\mathrm{SCR-MIN}}$ (A)	3.31	1.75	10.70	6.51	18.03	12.37	25.99	20.45

TABLE VI: Parameters for the generated Gaussian models and the preliminary testing of primary pads $\mathrm{Pri\_745\_705}$ to $\mathrm{Pri\_980\_995}$ with the sedan and SUV secondary pads.

	$\mathrm{Pri\_745\_705}$		$\mathrm{Pri\_745\_825}$		$\mathrm{Pri\_865\_910}$		$\mathrm{Pri\_980\_995}$	
Variable	Sedan	SUV	Sedan	SUV	Sedan	SUV	Sedan	SUV
a (A)	32.34	21.03	34.75	23.82	43.18	33.48	50.93	44.04
c (mm)	433	567	505	599	558	624	620	653
Pad width (mm)	704	704	826	826	911	911	996	996
P_{P} (mm)	704	704	826	826	911	911	996	996
$I_{\mathrm{SCR-MIN}}$ (A)	33.54	29.26	35.67	29.95	44.48	39.56	53.55	49.50

2332-7782 (c) 2016 IEEE. Personal use is permitted, but republication/redistribution requires IEEE permission. See http://www.ieee.org/publications_standards/publications/rights/index.html for more information.

This article has been accepted for publication in a future issue of this journal, but has not been fully edited. Content may change prior to final publication. Citation information: DOI 10.1109/TTE.2017.2666554, IEEE Transactions on Transportation Electrification

TABLE VII: $I_{\mathrm{SCR-MAX}}$, $I_{\mathrm{SCR-MIN}}$, $I_{\mathrm{SCR-AVG}}$ and δI_{SCR} for the primary pads Pri_745_705 to Pri_980_995 with the sedan and SUV secondary pads.

	Pri_745_705		Pri_745_825		Pri_865_910		Pri_980_995	
Variable	Sedan	SUV	Sedan	SUV	Sedan	SUV	Sedan	SUV
Chosen P_{P} (mm)	760	760	935	935	1327	1327	1557	1557
$I_{\mathrm{SCR-MAX}}$ (A)	35.33	28	37.01	28	43.49	34.20	51.12	44.34
$I_{\mathrm{SCR-MIN}}$ (A)	30.02	27.20	29.51	26.02	21	21.59	21	21.28
$I_{\mathrm{SCR-AVG}}$ (A)	32.67	27.60	33.26	27.01	32.24	27.89	36.06	32.81
δI_{SCR} (A)	5.31	0.80	7.49	1.98	22.49	12.61	30.12	23.06

TABLE VIII: Material usage for IPT highways based on the primary pads Pri_745_705 to Pri_980_995.

Variable	Pri_745_705	Pri_745_825	Pri_865_910	Pri_980_995
Ferrite mass per pad (kg)	10.91	13.34	16.97	21.02
Litz length per pad (m)	76.36	86.60	110.45	137.16
Number of pads per km	1316	1070	753	642
Ferrite mass per km (tonnes)	14.36	14.27	12.79	13.49
Litz length per km (km)	100.45	92.65	83.21	88.08

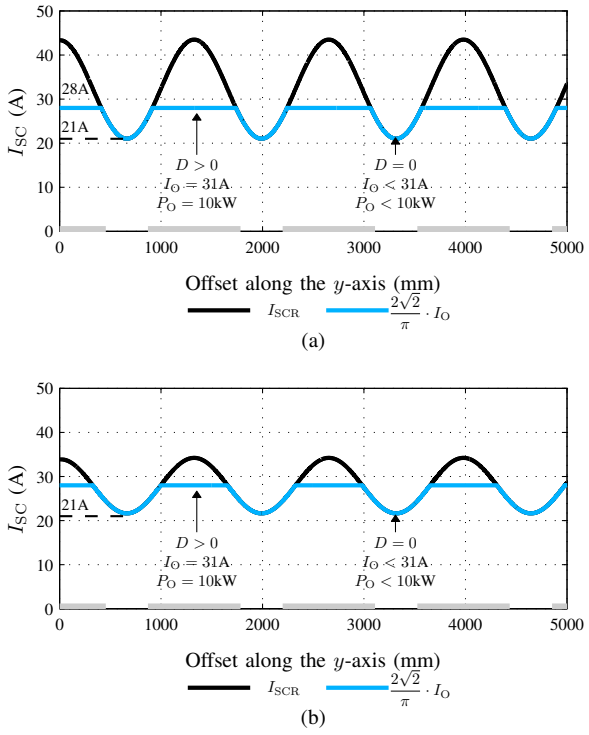

Fig. 13: Proposed IPT highway for the dynamic EV charging design example assuming the EV is perfectly aligned along the x-axis (e.g. $xos = 0$ mm). Highway uses Pri_865_910 primary pads placed with a pad pitch of 1327 mm to power the (a) sedan - Sec_465_495 (b) SUV - Sec_930_885 secondary pads.

When $I_{\mathrm{SCR}} > 28$ A, I_{O} is regulated to 30.77 A as the secondary controller switching duty cycle $D > 0$. Consequently, the 325 V EV battery can be charged at the desired 10 kW power level. On the other hand when $I_{\mathrm{SCR}} \leq 28$ A, then $D = 0$ and I_{O} falls and is given by $I_{\mathrm{O}} = \frac{\pi}{2\sqrt{2}} \cdot I_{\mathrm{SCR}}$. For this condition a reduced power output is transferred to the EV battery bank. As the minimum I_{SCR} for both EV classes in Fig. 13 is 21 A, or 75% of 28 A, the minimum power transferred to the EVs as they travel is thus 7.5 kW or 75% of 10 kW. Moreover, as the $I_{\mathrm{SCR-AVG}}$ for both classes is significantly greater than 28 A, the EVs will be charged at 10 kW for a large portion of their travel and this is evident from the I_{SC} profiles in Fig. 13.

This practical design example has shown the general approach for primary pad size selections for the dynamic charging of EVs along IPT highways. By adapting this approach, highways with differing power requirements or operating conditions can be designed with relative ease.

X. Conclusions

In this paper, an IPT highway was proposed to allow power transfer to EVs as they move. Such a highway would achieve this by sequentially energising multiple primary pads buried under the road surface when the vehicle pad is in proximity to receive power. As the cross coupling between the primary pads was found to be at most 5%, the pads can be energised independently with minimal energy transfer between adjacent primary pads. A window function (here fitted using a Gaussian distribution) was then created to model the I_{SC} profiles when individual primary pads are energised.

By considering the I_{SC} profiles due to each primary pad as phasors, an analytical expression was then developed that could predict the resultant I_{SC} from energising multiple primary pads depending on the phase angle (θ) between the

2332-7782 (c) 2016 IEEE. Personal use is permitted, but republication/redistribution requires IEEE permission. See http://www.ieee.org/publications_standards/publications/rights/index.html for more information.

This article has been accepted for publication in a future issue of this journal, but has not been fully edited. Content may change prior to final publication. Citation information: DOI 10.1109/TTE.2017.2666554, IEEE Transactions on Transportation Electrification

individual primary pad currents. From this phasor analysis, it was concluded that in order to maximise I_{SC} and hence power transfer, the primary pads in the highway should be energised with currents that are in phase with one another ($\theta = 0$ rad). When this condition is satisfied, the phasors add constructively and the resultant I_{SC} (or I_{SCR}) is simply the sum of the contributions from each primary pad.

Using these Gaussian models and the preceding phasor analysis, an analytical expression describing the expected power transfer for a highway based system was formed. An extension to the previous design example was then proposed to show how pads could be sized for practical dynamic applications as well. For this modified design example, it was shown that pads could be sized to allow 10 kW power transfer to sedans and SUVs with only a 25% reduction in power as they drive along the highway.

REFERENCES

[1] E. Grunditz and T. Thiringer, "Performance Analysis of Current BEVs - Based on a Comprehensive Review of Specifications," *IEEE Trans. Transport. Electrific.*, vol. PP, no. 99, pp. 1–1, 2016.

[2] S. S. Williamson, A. K. Rathore, and F. Musavi, "Industrial Electronics for Electric Transportation: Current State-of-the-Art and Future Challenges," *IEEE Trans. Ind. Electron.*, vol. 62, no. 5, pp. 3021–3032, May 2015.

[3] M. Yilmaz and P. T. Krein, "Review of Battery Charger Topologies, Charging Power Levels, and Infrastructure for Plug-In Electric and Hybrid Vehicles," *IEEE Trans. Power Electron.*, vol. 28, no. 5, pp. 2151–2169, May 2013.

[4] J. Du and M. Ouyang, "Review of electric vehicle technologies progress and development prospect in China," in *Proc. IEEE Electr. Veh. Symp. and Expo.*, Nov. 2013, pp. 1–8.

[5] S. G. Wirasingha and A. Emadi, "Classification and Review of Control Strategies for Plug-In Hybrid Electric Vehicles," *IEEE Trans. Veh. Technol.*, vol. 60, no. 1, pp. 111–122, Jan. 2011.

[6] V. Etacheri, R. Marom, R. Elazari, G. Salitra, and D. Aurbach, "Challenges in the development of advanced Li-ion batteries: a review," *J. Energy Environ. Sci.*, vol. 4, pp. 3243–3262, July 2011.

[7] J. M. Miller and A. Daga, "Elements of Wireless Power Transfer Essential to High Power Charging of Heavy Duty Vehicles," *IEEE Trans. Transport. Electrific.*, vol. 1, no. 1, pp. 26–39, Jun. 2015.

[8] M. Bojarski, E. Asa, K. Colak, and D. Czarkowski, "Analysis and Control of Multi-Phase Inductively Coupled Resonant Converter for Wireless Electric Vehicle Charger Applications," *IEEE Trans. Transport. Electrific.*, vol. PP, no. 99, pp. 1–1, 2016.

[9] S. Samanta and A. K. Rathore, "A New Current-Fed CLC Transmitter and LC Receiver Topology for Inductive Wireless Power Transfer Application: Analysis, Design, and Experimental Results," *IEEE Trans. Transport. Electrific.*, vol. 1, no. 4, pp. 357–368, Dec. 2015.

[10] S. Y. Choi, J. Huh, W. Y. Lee, and C. T. Rim, "Asymmetric Coil Sets for Wireless Stationary EV Chargers With Large Lateral Tolerance by Dominant Field Analysis," *IEEE Trans. Power Electron.*, vol. 29, no. 12, pp. 6406–6420, Dec. 2014.

[11] F. Y. Lin, C. Carretero, G. A. Covic, and J. T. Boys, "Reduced Order Modelling of the Coupling Factor for Varying Sized Pads Used in Wireless Power Transfer," *IEEE Trans. Transport. Electrific.*, vol. PP, no. 99, pp. 1–1, 2016.

[12] F. Y. Lin, G. A. Covic, and J. T. Boys, "Leakage Flux Control of Mismatched IPT Systems," *IEEE Trans. Transport. Electrific.*, vol. PP, no. 99, pp. 1–1, 2016.

[13] S. Lukic and Z. Pantic, "Cutting the Cord: Static and Dynamic Inductive Wireless Charging of Electric Vehicles," *IEEE Electrific. Mag.*, vol. 1, no. 1, pp. 57–64, Sept. 2013.

[14] S. Jeong, Y. J. Jang, and D. Kum, "Economic Analysis of the Dynamic Charging Electric Vehicle," *IEEE Trans. Power Electron.*, vol. 30, no. 11, pp. 6368–6377, Nov. 2015.

[15] G. A. Covic and J. T. Boys, "Modern Trends in Inductive Power Transfer for Transportation Applications," *IEEE J. Emerg. Sel. Topics Power Electron.*, vol. 1, no. 1, pp. 28–41, Mar. 2013.

[16] S. Li and C. C. Mi, "Wireless Power Transfer for Electric Vehicle Applications," *IEEE J. Emerg. Sel. Topics Power Electron.*, vol. 3, no. 1, pp. 4–17, Mar. 2015.

[17] J. P. K. Sampath, D. M. Vilathgamuwa, and A. Alphones, "Efficiency Enhancement for Dynamic Wireless Power Transfer System With Segmented Transmitter Array," *IEEE Trans. Transport. Electrific.*, vol. 2, no. 1, pp. 76–85, Mar. 2016.

[18] A. Zaheer, M. Neath, H. Z. Z. Beh, and G. A. Covic, "A Dynamic EV Charging System for Slow Moving Traffic Applications," *IEEE Trans. Transport. Electrific.*, vol. PP, no. 99, pp. 1–1, 2016.

[19] A. Kamineni, M. Neath, A. Zaheer, G. A. Covic, and J. T. Boys, "Interoperable EV detection for Dynamic Wireless Charging with Existing Hardware and Free Resonance," *IEEE Trans. Transport. Electrific.*, vol. PP, no. 99, pp. 1–1, 2016.

[20] Q. Zhu, Y. Zhang, C. Liao, Y. Guo, L. Wang, and L. WANG, "Null-Coupled Electromagnetic Field Cancelling Coil for Wireless Power Transfer System," *IEEE Trans. Transport. Electrific.*, vol. PP, no. 99, pp. 1–1, 2016.

[21] G. R. Nagendra, G. A. Covic, and J. T. Boys, "Determining the Physical Size of Inductive Couplers for IPT EV systems," *IEEE J. Emerg. Sel. Topics Power Electron.*, vol. 2, no. 3, pp. 571–583, Sept. 2014.

[22] M. B. Budhia, G. A. Covic, J. T. Boys, and C.-Y. Huang, "Development and evaluation of single sided flux couplers for contactless electric vehicle charging," in *Proc. IEEE Energy Conv. Congr. Expo. (ECCE)*, Sept. 2011, pp. 614–621.

[23] M. B. Budhia, J. T. Boys, G. A. Covic, and C.-Y. Huang, "Development of a Single-Sided Flux Magnetic Coupler for Electric Vehicle IPT Charging Systems," *IEEE Trans. Ind. Electron.*, vol. 60, no. 1, pp. 318–328, Jan. 2013.

[24] M. B. Budhia, G. A. Covic, and J. T. Boys, "Design and Optimisation of Magnetic Structures for Lumped Inductive Power Transfer Systems," in *Proc. IEEE Energy Conv. Congr. Expo. (ECCE)*, Sept. 2009, pp. 2081–2088.

[25] ——, "Design and Optimization of Circular Magnetic Structures for Lumped Inductive Power Transfer Systems," *IEEE Trans. Power Electron.*, vol. 26, no. 11, pp. 3096–3108, Nov. 2011.

[26] M. B. Budhia, "Improved Couplers for Charging Stationary and Moving Electric Vehicles," Ph.D. dissertation, Dept. Elect. and Comp. Eng., Univ. Auckland, Auckland, NZ, 2012.

[27] S. C. Chapra and R. P. Canale, *Numerical Methods for Engineers*, 5th ed. The McGraw-Hill Companies, 2006.

[28] G. R. Nagendra, J. T. Boys, G. A. Covic, B. S. Riar, and A. Sondhi, "Design of a double coupled IPT EV highway," in *Proc. IEEE Ind. Electron. Conf. (IECON)*, Nov. 2013, pp. 4606–4611.

[29] H. Hao, G. A. Covic, and J. T. Boys, "An Approximate Dynamic Model of LCL- T -Based Inductive Power Transfer Power Supplies," *IEEE Trans. Power Electron.*, vol. 29, no. 10, pp. 5554–5567, Oct. 2014.

[30] ——, "A Parallel Topology for Inductive Power Transfer Power Supplies," *IEEE Trans. Power Electron.*, vol. 29, no. 3, pp. 1140–1151, Mar. 2014.

[31] J. T. Boys, G. A. Covic, and Y. Xu, "DC Analysis Technique for Inductive Power Transfer Pick-Ups," *IEEE Power Electron. Lett.*, vol. 1, no. 2, pp. 51–53, June 2003.

Ganesh Nagendra (S'12-M'16) received his B.E. (Hons.) and Ph.D. from The University of Auckland, New Zealand, in 2011 and 2016 respectively.

His research interests include the design and analysis of inductive couplers and power electronics circuits to allow for the charging of electric vehicles (EVs) as they travel along inductive power transfer (IPT) highways.

2332-7782 (c) 2016 IEEE. Personal use is permitted, but republication/redistribution requires IEEE permission. See http://www.ieee.org/publications_standards/publications/rights/index.html for more information.

This article has been accepted for publication in a future issue of this journal, but has not been fully edited. Content may change prior to final publication. Citation information: DOI 10.1109/TTE.2017.2666554, IEEE Transactions on Transportation Electrification

Grant Covic (S'88-M'89-SM'04) received his BE (Hons), and PhD degrees in Electrical and Electronic Engineering from The University of Auckland (UoA), New Zealand in 1986 and 1993 respectively. He was appointed as a full time Lecturer in 1992, a Senior lecturer in 2000, an Associate Professor in 2007 and to Professor in 2013 within the Electrical and Computer Engineering Department at the UoA, New Zealand. In 2010 he co-founded (with Prof. John Boys) a new global start-up company HaloIPT focusing on electric vehicle (EV) wireless charging infrastructure, which was sold in late 2011. Presently he heads inductive power research at the UoA and co-leads the interoperability sub-team within the SAE J2954 wireless charging standard for EVs.

His research and consulting interests include power electronics, electric vehicle battery charging and highly resonant inductive (contact-less) power transfer (IPT) from which he has published more than 100 refereed papers in international journals and conferences. He holds a number of US patents with many more pending, from which licenses in specialized application areas of IPT have been granted around the world. He is a Fellow of the Institution of Professional Engineers New Zealand, a Fellow of the Royal Society of New Zealand, and (together with Prof. Boys) has been awarded the New Zealand Prime Ministers Science Prize, the KiwiNet Research Commercialisation Award, and the Vice Chancellors Commercialisation Medal for his work in IPT.

John Boys received the B.E, M.E., and Ph.D. degrees in Electrical and Electronic Engineering from the University of Auckland, New Zealand, in 1963, 1965 and 1968, respectively.

After completing his Ph.D. degree, he was with SPS technologies for five years before returning to academia as a Lecturer at the University of Canterbury, New Zealand. He moved to Auckland in 1977 where he developed his work in Power Electronics. He is currently a Distinguished Professor Emeritus at the University of Auckland in the Department of Electrical and Computer Engineering, and is co-founder of HaloIPT. He has published more than 100 papers in international journals and is the holder of more than 20 US patents from which licenses in specialized application areas have been granted around the world. His specialist research areas are power electronics and inductive power transfer.

Prof. Boys is a Fellow of the Royal Society of New Zealand and a Distinguished Fellow of the Institution of Professional Engineers New Zealand.

2332-7782 (c) 2016 IEEE. Personal use is permitted, but republication/redistribution requires IEEE permission. See http://www.ieee.org/publications_standards/publications/rights/index.html for more information.